JCTC Journal of Chemical Theory and Computation

On the Potential Use of Squaraine Derivatives as Photosensitizers in Photodynamic Therapy: A TDDFT and RICC2 Survey

Angelo Domenico Quartarolo,[†] Emilia Sicilia,[†] and Nino Russo*,[†]

Dipartimento di Chimica and Centro di Calcolo ad Alte Prestazioni per Elaborazioni Parallele e Distribuite-Centro d'Eccellenza MURST, Università della Calabria, I-87030 Arcavacata di Rende, Italy

Received April 23, 2009

Abstract: A time-dependent density functional theory (TDDFT) and the second-order approximated coupled-cluster model with the resolution of identity approximation (RICC2) studies are reported here for some classes of squaraine derivatives. These compounds have a sharp electronic band, ranging from the visible to near-red part of the spectrum, with an high molar absorption coefficient. These features make them potential photosensitizers in the photodynamic therapy of cancer (PDT), in which a light source, a photosensitizer, and molecular oxygen ($^3O_2$) are combined to give cytotoxic singlet oxygen ($^1O_2$) as a final result in a photochemical process. For the examined structures, the introduction of different substituents (electron donating, electron withdrawing, or fused rings) in the parent molecule, in order to give different squaraine derivatives, changes the maximum absorption wavelength (λ_{max}) from 620 to 730 nm, giving a near-red absorbing photosensitizer that can better penetrate human tissue to damage tumor cells. Theoretical results, obtained from both TDDFT/PBE0 and RICC2, are able to reproduce qualitatively the substitution effect on λ_{max}, resulting in a useful tool for testing different structure modifications and, in general, for the molecular design of PDT photosensitizers. Calculated vertical excitation energies (singlet−singlet transitions) generally agree with experimental data within 0.3 eV. The singlet oxygen generation ability of these compounds requires that their triplet energy, for a type II reaction mechanism, should be greater than 0.98 eV. Theoretical triplet energies from the RICC2 method suggests that this requisite is fulfilled for all compounds, though the results are generally overestimated with respect to experiment by 0.7 eV, whereas TDDFT/PBE0 triplet energies, which are underestimated within 0.2 eV in few cases, lie close to the above-mentioned limit and can be considered suitable for PDT applications.

1. Introduction

Squaraine dyes are a class of organic compounds derived from the 1,3-condensation reaction between squaric acid and electron-rich compounds and are characterized by a sharp and intense electronic absorption band in the near-red part of the visible region (600−700 nm).[1,2] Recently, these compounds have been investigated for use in many research areas, for example, technological applications, such as dye-sensitized solar cells,[3] optical storage devices,[4] and fluorescent probes for detecting metal ions[5,6] and in photosensitizer drugs in photodynamic therapy of cancer (PDT).[7−9] This latter application is a noninvasive medicine treatment for different tumoral diseases, like skin or bladder cancer, or for psoriasis and age-related macular degeneration.[10−14] The basic principle of PDT is given by an appropriate combination of a light source, a chemical dose containing photosensitizer molecules and dioxygen, that is largely present in the human cell environment and can promote selective cellular

* Corresponding author: Telephone: +39-0984-492048. Fax: +39-0984-492044. E-mail: nrusso@unical.it.

[†] Università della Calabria.

10.1021/ct900199j CCC: $40.75
Published on Web 06/25/2009

damage through irradiation.[15] There are two reaction mechanisms through which the photosensitizer drug can produce a cytotoxic effect against cancer cells.[16−19] The first pathway, the so-called type I mechanism, involves radical oxygen species generated, for example, from an electron transfer between a photosensitizer in an excited state and an organic substrate followed by the interaction with dioxygen. In the second mechanism, or type II mechanism, the photosensitizer is promoted by irradiation to its first singlet excited state (S_1) and then a fast depletion from this state, via an intersystem spin crossing decay, to the first excited triplet state (T_1) occurs. An energy transfer process can occur between the photosensitizer T_1 state and ground-state molecular oxygen ($^3O_2$) leading to the formation of singlet molecular oxygen ($^1O_2$), which represents the final cytotoxic agent.[20] One of the main features for an optimal molecule to act as a type II PDT drug is the presence of an intense electronic absorption band in its spectrum, falling inside the therapeutic window (600−900 nm), where tissue penetration by light is greater. This goal is usually achieved by further extending the electronic delocalization of π-molecular systems and/or by introducing suitable functional groups in order to reduce the HOMO−LUMO energy gap and shifting the electronic absorption band in the near-red part of the visible spectrum.[21] On the other hand, the efficiency of the intersystem spin crossing mechanism is enhanced by the presence of heavy atoms, for example, bromine or transition metals, that as a result of spin−orbit effects increase the triplet quantum yield. Moreover, other important experimental factors affect the efficiency of a PDT photosensitizer such as high singlet oxygen quantum yield, long triplet state lifetime, and water solubility, as they have to work in biological systems, low dark toxicity, and preferential localization in the tumoral tissue.[15] Photosensitizers, currently investigated for PDT applications, belong mainly to the class of porphyrin-like systems (e.g., expanded porphyrins, phthalocyanine, and porphycene derivatives)[22] or, in part, to nonporphyrin systems (e.g., psoralens, and phenothiazines dyes).[23] Photofrin, a porphyrin derivative, has been approved in many countries for the treatment of early stage lung cancer.[24,25] Currently, other polypyrrolic macrocycles as lutetium texaphyrin (Lutex),[26] an expanded metal porphyrin-like molecule, or a benzoporphyrin derivative (Verteporphyrin)[27] are in different stages of clinical trials. Recently, many studies have regarded the synthesis and photochemical characterization of new nonporphyrin systems for PDT application. Some examples are given by difluoro-boron(III) dipyrromethenes,[28,29] green perylenediimides,[30] and squaraine dyes.[31] Previous works regarding the synthesis, photophysical properties, and in vitro biological studies of halogenated (brominated and iodinated) squaraine dyes by Ramaiah et al. proved the DNA damage through singlet oxygen generation and that it takes place, for the nonhalogenated form, through the type I mechanism.[32] For these compounds, which exist in solution as either neutral or protonated forms depending on the pH, the maximum absorbance wavelength falls in the range of 500−600 nm. Moreover, the influence of heavy atom on singlet oxygen generation has been studied also, for example, in works concerning squarilium cyanine dyes containing sulfur and selenium[33] or in iodinated squaraine-rotaxanes derivatives.[34] In this theoretical work we will focus our attention on two series of symmetrical squaraine derivatives (Scheme 1 and 2), synthesized in the past few years by Bonnett et al.[35] and Beverina et al.[36] These compounds have been specifically designed to further red-shift the maximum absorption wavelength by the addition of different functional groups and to increase the solubility in water.[36] Structures and electronic spectra of these two series of compounds have been calculated by means of density functional theory (DFT) and its time-dependent formulation (TDDFT)[37] as well as by the second-order approximated coupled-cluster model with the resolution of identity approximation (RICC2).[38] The main aim of this work was to reproduce the electronic band changes as a function of the substituent groups and to evaluate the triplet energy of each molecule, which is a basic requirement in order to consider it as a type-II PDT photosensitizer.

Scheme 1. Two-Dimensional Plot for Structures 1a−e, 2, and 3a−b

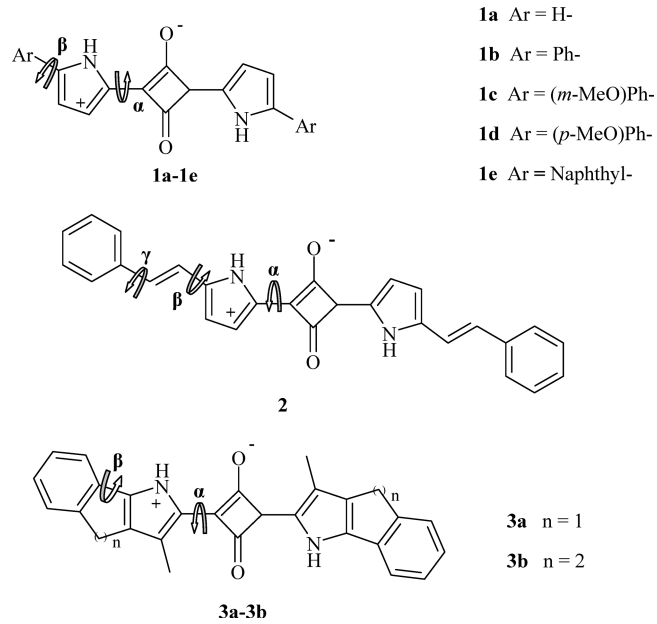

2. Computational Details

The TURBOMOLE V5.10 software package has been used for the TDDFT and RICC2 calculations.[39] Geometry optimizations, without imposing symmetry constraints, as well as vibrational frequency analysis were carried out at the density functional level of theory in conjunction with the nonempirical PBE0 hybrid functional that adds up a fixed amount of Hartree−Fock exchange energy (25%) to the gradient corrected PBE exchange correlation functional.[40,41] The split valence basis set plus polarization functions (SVP) of Ahlrichs et al.[42] was used for all atoms for the structure optimizations and vibrational frequency analysis. Vertical excitation energies were calculated by means of two different methodologies: time-dependent density functional linear response theory (TD-DFRT)[38,43] and RI-CC2.[38,44,45] In both cases, singlet and triplet vertical transitions for each molecule were obtained starting from the PBE0/SVP optimized

Scheme 2. Two-Dimensional Plot of Structures 4a−c, 5a−b, and 6

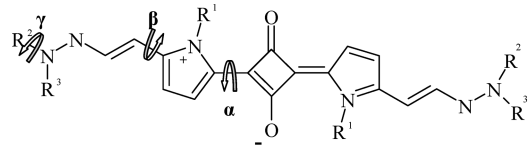

4a $R^1 = CH_3$ $R^2 = R^3 = Ph$

4b $R^1 = CH_3$, $R^2 = R^3 = CH_3$

4c $R^1 = CH_3$, $R^2 = H$, $R^3 = p$-Br-Ph

4a-4c

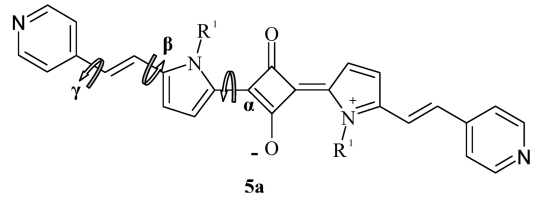

5a

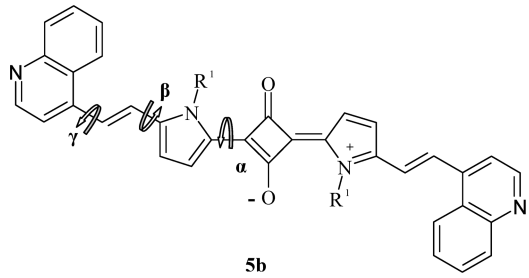

5b

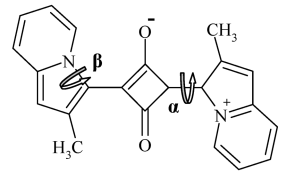

6

structures. In order to assess the influence of the chosen basis set upon excitation energies for TD-DFT calculations, different quality basis sets, with an increasing number of basis functions, were initially tested on molecule 6. For this aim the following basis sets were employed: split valence basis sets without and with polarization functions on hydrogen atoms (SV(P) and SVP),[42] double- and triple-ζ valence basis set plus one (DZP and TZVP)[46] and two polarization functions for each atom (TZVPP)[46] and the correlated consistent polarized valence double and triple-ζ basis sets of Dunning et al. (cc-pVDZ, cc-pVTZ).[47] The latter have been employed also with the addition of s and p diffuse functions (aug-cc-pVDZ and aug-cc-pVTZ). The reliability of excitation energies of organic and inorganic dyes, obtained from the adopted split valence basis set (SVP) and hybrid functional (PBE0), has been also proved in recent works and yields a mean absolute error (MAE) within 0.3−0.4 eV.[48−51] For RICC2 singlet and triplet excitation energy calculations, only SVP and TZVP basis sets have been tested, since the basis sets increasing size becomes more computationally demanding. In this case, single point calculations were made on PBE0/SVP optimized geometries. The influence of solvent effects on geometries and excitation energies has been estimated with the COSMO (conductor-like screening model) approach,[52,53] where the solute molecule is embedded within a dielectric of permittivity ε, that represents the solvent. The inclusion of bulk solvent effects can quantitatively improve excitation energies, though in vacuo results qualitatively account for the observed experimental trends. The dielectric constant values of chloroform ($\varepsilon = 4.9$, for compounds 4a−c, 5a−b and 6) and dichloromethane ($\varepsilon = 8.93$, for compounds 1a−e, 2, 3a−b) and default parameters for the cavity generation have been used for solvent calculations.

3. Results and Discussion

3.1. Structures. Two classes of squaraine derivatives have been studied in this work. In the first series (see Scheme 1), synthesized and characterized by Bonnett et al.,[35] suitable substituent groups are introduced in the position 2 of the pyrrole moieties in order to red-shift the λ_{max} with respect to the parent molecule 1a. The reported molecules include electron-donating phenyl (1b), phenyl substituted or naphthyl groups (1c, 1d and 1e), styryl substituent containing a phenyl terminal group (2a), and saturated 5- and 6-term rings between the benzenoid and pyrrole parts (3a−b). In the second series, we have considered the squaraine derivatives (see Scheme 2), synthesized by Beverina et al.,[36] where the pyrrole parts were functionalized by arylhydrazone groups (4a−c) or, as for the case of 2a, by extending the π conjugation system with heteroaromatic rings, specifically a pyridine molecule for 5a and a quinoline ring in 5b, and last through an indolizine ring attached directly to the squaric core structure (6). All reported structures (see Figures 1 and 2 in the Supporting Information) have been considered to assume an *anti* geometry configuration on the basis of

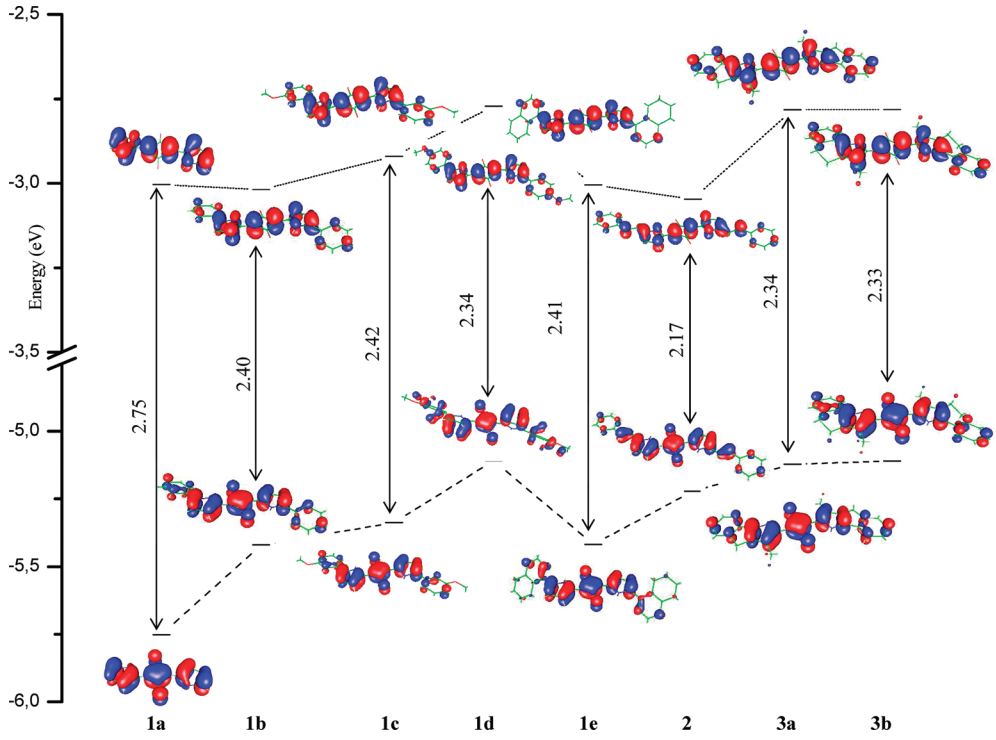

Figure 1. HOMO and LUMO isodensity molecular surfaces and energy level diagram for 1a−e, 2 and 3a−b.

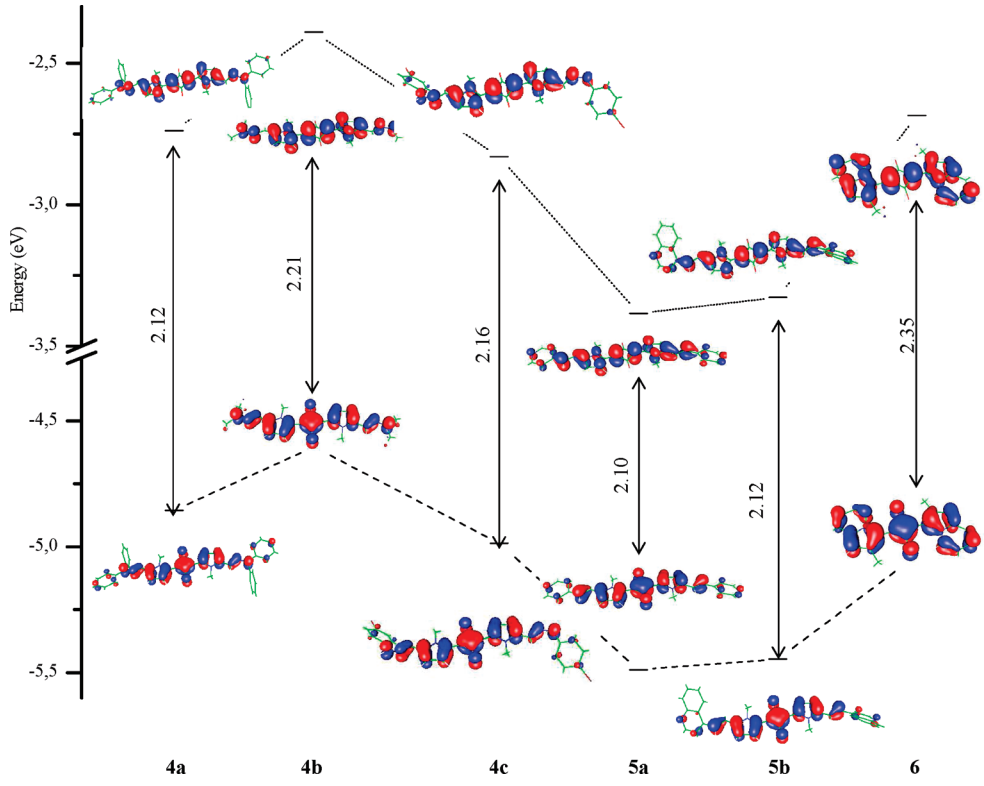

Figure 2. HOMO and LUMO isodensity molecular surfaces and energy level diagram for 4a−c, 5a−b and 6.

preliminary calculations on 1a and 6 compounds. In fact, after geometry optimizations, this conformation resulted to be energetically more stable than the corresponding *syn* geometries, even if by few kcal/mol energy units (including zero-point vibrational correction energies). The stabilization is mainly due to two reasons: (a) the formation of two intramolecular hydrogen bonds between the pyrrole hydrogen atoms and the oxygen atoms; and (b) the steric hindrance effects. The possible deviation from planarity of all compounds has been analyzed by defining three main dihedral angles (α, β, and γ) as reported in Schemes 1 and 2. The dihedral angle α connects the pyrrole ring to the squaric part through the carbon−carbon bond, which showed theoretically a partial double character (∼1.38−1.40 Å). The dihedral angle β represents the distortion between the substituent group at position 2 of the pyrrole ring and the ring itself or,

Table 1. Dihedral Angles α, *β*, *γ*, as Indicated in Schemes *1* and *2*

molecule	dihedral angles α	*β*	*γ*
1a	0.0	–	–
1b	0.2	14.4	–
1c	0.1	17.0	–
1d	0.1	13.2	–
1e	0.6	37.7	–
2	1.0	3.5	4.2
3a	0.9	0.2	–
3b	0.5	12.4	–
4a	1.5	176.1	95.2 (5.8)[a]
4b	1.5	179.3	5.0
4c	2.3	174.5	37.1
5a	1.1	176.1	4.9
5b	0.5	171.2	35.2
6	0.0	0.0	–

[a] Dihedral angles for the two phenyl groups.

in the case of the condensed structures (3a−b and 6), the degree of coplanarity of the fused rings. For structures 2 and 5a−b, the elongation of the electronic delocalization through the formation of carbon−carbon or nitrogen−carbon bonds with the presence of a terminal heteroaromatic ring gives rise to another degree of conformational freedom represented by the dihedral *γ*. The dihedral angle values (α, *β*, and *γ*) for each molecule are summarized in Table 1. In all compounds, the squaric core part is nearly coplanar with the *N*-substituted pyrrole ring (α value is lesser than 3°). The dihedral *β* angle depends on the nature of the substitution on the pyrrole rings. For compounds 1b−e, which a phenyl (substituted) or naphthyl ring is bound to the pyrrole one, the deviation ranges between 13° and about 40° (Table 1), depending on the different steric hindrance of the substituent group. For compounds reported in Scheme 2 and compound 2, which present a chain elongation starting from the position 2 of the pyrrole ring, the *β* value (−N−C−C−N− or −N−C−C−C−) denotes a planar conformation for this part of the molecules. Condensed structures are strictly coplanar except for compound 3b where the cyclohexenyl ring has a *β* value equal to 12.4°. Further substitution along the molecular chain, represented by the dihedral angle *γ*, is relevant in the case of hindered substituent groups (4c and 5b, *γ* values ca. 37° and 35°) or in situations where there are two adjacent phenyl groups, as is the case of 4a, which has two different *γ* values (95° and 6°) in order to minimize sterical repulsion between phenyl rings. The nature of the substituent groups as well as distortion from planarity can influence the electronic delocalization and, as a consequence, the λ_{max} value, as shown in the next paragraph.

3.2. Electronic Spectra. The electronic spectra of 2,4-bis-pyrrolyl squaraine derivatives are characterized, in the visible part of the electromagnetic spectrum, by a sharp and intense absorption band due to the *π* electronic system, which is highly delocalized. Formally the core part of these compounds can be described by three resonance structures with 12 *π*-electrons and a positive charge delocalized through the two symmetrical moieties. For all compounds UV−vis spectra are available;[35,36] moreover, for the compounds reported in Scheme 2, singlet oxygen quantum yield measurements and two-photon spectroscopical studies were also made.[31,36] In this section, we will outline the results obtained by TDDFT calculations of the λ_{max} in vacuo and in solvent environments and outline how structural changes are theoretically reproduced in comparison to the experimental behavior, also using more refined methodology as coupled-cluster methods. The basis set influence on λ_{max} was tested for compound 6, the results are reported in Table 2 and are relative to PBE0 calculations. It is evident that the increasing size of the basis set improves little the agreement with the experimental λ_{max} (684 nm), even by using the augmented triple-*ζ* basis set of Dunning et al.[47] In terms of eV units, the benefit is 0.04 and is well below the TDDFT method error deviation, which is typically within 0.4 eV.[48−50] So a good compromise between computational timings and numerical reproduction of λ_{max} can be obtained by just employing a SVP. Similar consideration can be made for the influence of the basis set on λ_{max} for the RICC2 methodology. In fact, from Table 2, it is evident that with this method the SVP basis sets also give results that differ by about 10 nm from that obtained by using the triple-*ζ* valence basis set. The excitation energies (in eV and nm) and oscillator strengths for the two series of squaraine derivatives (Scheme 1 and 2) obtained at both TDDFT and RICC2 level of theory in vacuo and in the presence of the solvent (TDDFT only) are reported in Table 3. All structures showed one excitation energy in the visible region composed mainly by a transition from the highest occupied molecular orbital (HOMO) to the lowest unoccupied one (LUMO). We will first analyze in vacuo TDDFT results. Considering the compound 1a as a reference structure for the evaluation of the λ_{max} shift as a function of substituents, it can be noted that the introduction of an electron-donating group (1b−e) increases the λ_{max} by 80−90 nm. Comparing the two isomeric forms 1c and 1d, the latter resulted more wavelength red-shifted by 18 nm as can be confirmed also by the experimental difference between the two isomers. This different behavior can be explained taking into account the energetic trend and the isodensity electron density surfaces of the HOMO (*π* orbital character) and LUMO (*π** orbital character) orbitals (see Figure 1). The molecular orbitals considered are those mainly involved in the electronic transition that gives rise to the maximum wavelength absorption band.

Table 2. Basis Set Influence for the First Excitation Energy Δ*E* (eV, nm) and Oscillator Strength *f* of Compound 6 from TDDFT and RICC2 Calculations

basis set	TDDFT[a] Δ*E*, eV	Δ*E*, nm	*f*	RICC2[a] Δ*E*, eV	Δ*E*, nm	exptl.[b] Δ*E*, eV	Δ*E*, nm
SV(P)	2.22 (2.08)	559	0.9762	2.08	596	1.81	684
SVP	2.22 (2.08)	559	0.9770	2.08	597		
DZ	2.20	563	0.9741				
DZP	2.21	560	0.9685				
TZVP	2.20	564	0.9736	2.04	607		
TZVPP	2.20	565	0.9579				
cc-pVDZ	2.22	559	0.9635	2.08	595		
cc-pVTZ	2.20	563	0.9585	2.05	605		
aug-cc-pVDZ	2.19	567	0.9560	2.04	609		
aug-cc-pVTZ	2.18	568	0.9548	2.02	612		

[a] Single point calculations from PBE0/SVP optimized structures. [b] In dichloromethane; from reference 36.

Table 3. Calculated Singlet Excitation Energies ΔE (eV and nm (in parentheses)) and Oscillator Strength f for All Studied Compounds[a]

	TDDFT,[b] vacuum		TDDFT,[b] c-pcm		RICC2,[b] vacuum	
molecule	ΔE	f	ΔE	f	ΔE	exptl.[c]
1a	2.73 (454)	0.832	2.78 (445)	0.909	2.61 (475)	/
1b	2.33 (533)	1.578	2.35 (528)	1.714	2.31 (537)	2.00 (621)
1c	2.33 (531)	1.661	2.35 (527)	1.792	2.31 (537)	1.98 (625)
1d	2.26 (549)	1.835	2.26 (548)	1.983	2.24 (552)	1.93 (643)
1e	2.27 (546)	1.701	2.28 (543)	1.803	2.29 (542)	2.02 (613)
2	2.12 (586)	2.368	2.14 (580)	2.526	2.16 (574)	1.84 (673)
3a	2.28 (544)	1.849	2.31 (537)	1.950	2.23 (555)	1.90 (654)
3b	2.25 (552)	1.746	2.27 (546)	1.840	2.22 (559)	1.88 (660)
4a	2.04 (609)	2.619	2.03 (611)	2.750	2.01 (616)	1.70 (728)
4b	2.24 (553)	2.029	2.23 (556)	2.228	2.18 (569)	1.80 (688)
4c	2.09 (593)	2.337	2.09 (593)	2.506	2.11 (586)	1.73 (717)
5a	2.07 (600)	2.356	2.12 (586)	2.516	2.13 (581)	1.83 (678)
5b	2.03 (612)	2.376	2.07 (600)	2.520	2.12 (585)	1.80 (688)
6	2.22 (559)	0.9770	2.26 (549)	1.033	2.08 (593)	1.81 (684)
MAE	0.31		0.32		0.30	

[a] In vacuo and solution (C-PCM) from TDDFT and in vacuo from RICC2 calculations. The mean absolute deviation (MAE) for excitation energies relative to TDDFT (in vacuo and solution) and RICC2 methods are given in eV. [b] Single point calculations from optimized structures at PBE0/SVP level of theory. [c] In chloroform for 1a−e, 2, and 3a−b; in dichloromethane for 4a−c, 5a−b, and 6.

The HOMO orbital for all compounds is characterized by an high electron density in the squaric core part, while for the LUMO orbital, electronic density is depleted from the oxygen atoms. By viewing the HOMO and LUMO orbital energies of 1d, both resulted destabilized with respect to 1c, but the LUMO is less destabilized in energy than the HOMO by ca. 0.1 eV, so λ_{max} increases. As can also be seen in Figure 1, oxygen electronic density belonging to the *m*-methoxy group in 1c is not involved in the electronic delocalization system. Moreover, the *m*-methoxy substitution in 1c leaves λ_{max} practically unchanged in comparison to the phenyl substituted case 1b (533 vs 531 nm), in qualitative agreement with the experimental values (621 vs 625 nm). Going to the next compound in Table 3, it can be seen that in 1e, the introduction of the naphthyl substituent group on the pyrrole ring, notwithstanding its strong electron-donating character, decreases slightly the value of λ_{max} (546 nm) with respect to 1d (549 nm), in qualitative agreement with the experimental λ_{max} trend. For 1e, the HOMO−LUMO energy gap is lower than that of 1d by 0.07 eV, the decreased λ_{max} could be due to the more distorted structure ($\beta = 38°$) which, therefore, reduces the overlapping of the molecular orbitals and a greater HOMO energy stabilization with respect to the LUMO orbital energy. The elongation of the molecular chain through a carbon−carbon double bond with a terminal phenyl group (compound 2) increases λ_{max} (586 nm). This fact is consistent with the experimental red-shift evidence and the decreasing of the HOMO−LUMO gap characterized by a strong energy destabilization of the HOMO orbital by ca. 0.2 eV with respect to 1e analogue orbital (see Figure 2). As for compounds of Scheme 1, the main results regarding the first lowest excitation energy (λ_{max} and oscillator strength) are summarized in Table 3. For the condensed ring structures (3a−b), theoretical λ_{max} are both red-shifted in comparison with the phenyl substituted form 1b with values, respectively, of 544 and 553 nm. In particular compound 3b, containing a six-term ring, is more red-shifted than 3a in agreement with the experiment. However, for these condensed structures, λ_{max} is lower in comparison to the more extended form 2, confirming that elongation is a better strategy for red-shifting of λ_{max}. The HOMO−LUMO energy gap trend for 3a−b also is consistent with TDDFT excitation energies and confirmed by experiment. For the compounds just examined, the oscillator strengths, corresponding to the spin- and dipole-allowed electronic transition in the visible range between 0.832 (1a) and 2.368 (2), the deviation of the calculated λ_{max} from the experimental one has a minimum value for 1e (0.25 eV) and a maximum value for 3a (0.38 eV). Proceeding to the second series of squaraine derivatives (see Scheme 2), we can note some structural differences and analogies with compounds in Scheme 1. In compounds 4a−c, the electronic delocalization was obtained by functionalizing the pyrrole ring by aryl- or alkyl-hydrazone groups. In this study, the nitrogen pyrrole atoms are always attached to a methyl group, although compound 4a was synthesized also with the group R^1 (see Scheme 1) constituted by a triethyleneglycolic chain in order to increase water solubility. Similarly for compounds 4b and 5a−b, the latter being synthesized only in this functionalized form, we adopted methyl groups as R^1 substituents. This choice was justified by the fact that a preliminary calculation for the evaluation of λ_{max} of compound 4a showed that its λ_{max} is unaffected if R^1 is present as a methyl or triethyleneglicolic group, as clearly evidenced also by experimental data. Analyzing first the squaraine derivatives containing arylhydrazone groups (4a−c), we noted that the highest calculated λ_{max} (609 nm) corresponds to compound 4a for which R^1 and R^2 terms are both electron-donating phenyl groups. The presence of weak electron-donating methyl groups in 4b gave a decreased value of λ_{max} (553 nm), whereas the situation represented by compound 4c, where R^2 is given by an hydrogen atom and R^3 by a *para*-bromine substituted phenyl group, is intermediate between that of 4a and 4b ($\lambda_{max} = 593$ nm). These results reflect the order of the HOMO−LUMO energy gaps depicted in Figure 2, the lowest energy gap (highest λ_{max}) corresponds to compound 4a (2.12 eV). In compounds 5a and 5b, the electron conjugation is extended from each pyrrole ring through a carbon−carbon double bond with, respectively, a pyridine and a quinoline terminal group (see Scheme 2). Experimentally the introduction of these weak electron-withdrawing heteroaromatic groups has the effect to reduce λ_{max} (678 nm for 5a, 688nm for 5b) with respect to the case of 4a, which contains strong electron-donating phenyl groups.

From TDDFT results, we note that the relative magnitude order and difference of λ_{max} 5a and 5b is well reproduced, and the maximum deviation of λ_{max} from the experimental data is 0.24 eV. Despite these results, by comparing compounds 4a and 4c (containing phenyl groups) with 5a−b, the experimental decrease of λ_{max} is not so clearly found from TDDFT excitation energies. Oscillator strengths of compounds 4a−c and 5a−b are in the range between 2.0 and 2.6 and generally more intense than the first series of squaraine derivatives (1a−e, 2, and 3a−b). In compound 6, the annelated structure, resulting from the further π-delocalization of the pyrrole ring, gives a calculated λ_{max} of 559 nm, which, among all examined compounds, presents the maximum energy difference from the experimental (about 0.4 eV). In this case, RICC2 calculations (see Table 3) gives an improved calculated λ_{max} with respect to the experimental value (593 vs 684 nm). The correlation of λ_{max} with the dihedral angle α (Scheme 2, compound 6), for both sides of the squaric core part, has been examined in order to verify if TDDFT deviation of λ_{max} stems from the simultaneous presence at room temperature of the different conformers. The next most stable conformer was found to be the *syn* conformer (2.7 kcal/mol above in energy) with λ_{max} identical (2.21 eV) to that of the *anti* conformer. The weighted contribution of λ_{max} to other conformers can be neglected on the basis of their higher energy (>20 kcal/mol) with respect to the *anti* energy minimum structure. For compound 6, where the π-system is more delocalized, it seems that RICC2 method better describes the electronic transition contribution of the double excitation character, which completely lacks in the TDDFT method. From our calculations, the percentage weight of these transitions is about 10%. However, in all the other cases, the difference of calculated λ_{max}, between TDDFT and RICC2 methods, is not so drastic, changing from in 0.02 to 0.08 eV (absolute values). Taking into account solvent effects through the C-PCM method, similar consideration holds for the excitation energies (no drastic changes in λ_{max}), while oscillator strengths are intensified in value (see Table 3). A quantitative assessment of the reliability of TDDFT and RICC2 results can be made by considering the mean absolute error (MAE) for the whole series of studied compounds. The value of MAE is nearly 0.3 eV (Table 3), so in this case, there is not an evident difference between the theoretical results obtained from both methodologies.

3.3. Triplet Energies. As pointed out in the Introduction, in oxygen-dependent type II reactions, the efficiency of a PDT photosensitizer drug is measured by its single oxygen quantum yield. The energy transfer from the triplet state of the photosensitizer to the ground-state molecular oxygen, in order to be an efficient process, needs an appropriate triplet energy for the photosensitizer. This value should be equal or greater to 0.98 eV, which corresponds to the experimental triplet molecular oxygen energy (or $^3\Sigma_g \rightarrow {}^1\Delta_g$ electronic transition). For compounds 4a−c, 5a−b and 6 also have been previously reported, a qualitative comparative study has been reported on their ability to generate singlet oxygen, by monitoring the time disappearance of the absorption band at 415 nm of 1,3-diphenylisobenzofuran, which can react with a photosensitizer dye to form an endoperoxide species. The experimental results proved that the above-mentioned compounds and in particular 4a and 4c (containing bromine atoms) are able to give a singlet oxygen yield. Triplet energies can be theoretically calculated from TDDFT and RICC2 methodologies as triplet excitation energies referred to the singlet ground state. As reported in the results of Table 4, the TDDFT computations indicate that all the studied compounds have triplet energies below the limit of 0.98 eV. In particular, in vacuo triplet energies are in the range between 0.61 (5b) and 0.95 eV (1a). Bulk solvation effects slightly increase the triplet excitation energies by 0.02−0.08 eV. It can be argued, from TDDFT, that only 1a−e, 3a−b, and 6 compounds lie close to the mentioned energetic gap. On the other hand, RICC2 calculations showed that for the studied compounds the triplet energies are between 1.13 (5a) and 1.36 eV (1a), fulfilling one of the requirements to act as a PDT drug. In order to better understand the origin of this great discrepancy between TDDFT and RICC2 results, we have studied a series of molecular systems where the triplet energies have been experimentally evaluated.[54−56] The results, collected in Table 5, clearly showed that the vertical triplet energies, from RICC2 calculations, are overestimated by about 0.6−0.7 eV in comparison with experimental results obtained from phosphorescence spectra, whereas the TDDFT triplet energies, from PBE0

Table 4. Triplet Energies in Vacuo and with C-PCM Solvation Model from TDDFT and in Vacuo from RICC2 Calculations

	TD-DFT[a]		RICC2[a]
molecule	ΔE, vacuum	ΔE, c-pcm[b]	ΔE, vacuum
1a	0.95	1.00	1.36
1b	0.85	0.88	1.28
1c	0.86	0.89	1.28
1d	0.85	0.87	1.27
1e	0.86	0.90	1.29
2	0.69	0.72	1.18
3a	0.87	0.90	1.28
3b	0.84	0.88	1.28
4a	0.65	0.70	1.18
4b	0.69	0.72	1.18
4c	0.65	0.71	1.17
5a	0.58	0.66	1.13
5b	0.61	0.69	1.15
6	0.91	0.96	1.27

[a] Single point calculations from optimized structures PBE0/SVP. [b] In chloroform ($\varepsilon = 4.9$) for 1a−e, 2, and 3a−b; in dichloromethane ($\varepsilon = 8.93$) for 4a−c, 5a−b, and 6.

Table 5. Triplet Energies $\Delta E_{S_0 - T_1}$ (eV) for Some Aromatic Hydrocarbons and the Free Base Porphyn (FBP) from TDDFT (PBE0) and RICC2 Calculations in Comparison with Experimental Values

	$\Delta E_{S_0 - T_1}$ (eV)		
molecule	PBE0[a]	RICC2[a]	exptl.[b]
benzene	3.68	4.42	3.69
naphthalene	2.65	3.35	2.65
anthracene	1.72	2.42	1.82
pyrene	2.05	2.71	2.08
FBP	1.38	2.24	1.58

[a] Single point calculations with TZVP basis set from PBE0/TZVP optimized geometries. [b] Experimental data taken from ref 54, except for FBP from refs 55 and 56.

calculations, are slightly underestimated, the maximum deviation being 0.2 eV for the free base porphyn.

4. Conclusions

In this paper, the theoretical electronic spectra in the visible region for some classes of squaraine derivatives have been simulated by adopting two approaches: time-dependent density functional methods (TDDFT) and coupled-cluster model with the resolution of identity approximation (RICC2). First, the geometrical structures corresponding to energy minima have been examined and, in particular, their possible conformational dihedral changes that can affect the maximum absorption wavelength, due to more or less effective molecular orbital overlapping. For example, for naphthyl substituted squaraine (1e), the presence of strong electron-donating gives λ_{max} a decreased value with respect to the phenyl substituted counterpart, as a consequence of the distortion (about 40°) from the planarity of the rest of the molecule. The maximum absorption wavelength shifts, as a function of the substituent nature within each different class of squaraine derivatives, are qualitatively well reproduced in comparison with experimental results by the two theoretical approaches. By comparing the two theoretical approaches, singlet excitation energies show, for both TDDFT and RICC2 results, an absolute mean error of roughly 0.3 eV. In this case, their performance in predicting electronic spectra is comparable. On the other hand, triplet energies calculated by RICC2 are strongly overestimated (about 0.7 eV) with respect to the experiment than those obtained by PBE0 calculations. All studied compounds show an absorption electronic band that falls in the so-called therapeutic window (550−800 nm) for PDT treatment. Notwithstanding, including bulk solvation effects, only a few compounds (1a−e, 3a−b, and 6) have a triplet energy close to that of molecular oxygen and, consequently, could be active as type II PDT photosensitizers. The limits of hybrid functionals in TDDFT are currently under investigation through the development of new DFT functionals (so-called long-range corrected hybrid functionals) in order to improve the accuracy of excitation energies, in particular, for charge transfer electronic transitions where TDDFT gives unreliable results.[57−59]

Acknowledgment. Financial support from the Università degli Studi della Calabria and Regione Calabria (POR Calabria 2000/2006, misura 3.16, progetto PROSICA) is gratefully acknowledged.

Supporting Information Available: All in vacuo optimized structures with Cartesian coordinates for all compounds reported in Scheme 1 and 2. This material is available free of charge via the Internet at http://pubs.acs.org.

References

(1) Schmidt, A. H. In *Oxocarbons*, West, R. Ed.; Academic Press: New York, 1980; pp 1−185.

(2) Law, K. J. *Chem. Rev.* **1993**, *93*, 449–486.

(3) Yum, Jun-Ho; Walter, P.; Huber, S.; Rentsch, D.; Geiger, T.; Nüesch, F.; De Angelis, F.; Grätzel, M.; Nazeerudin, M. K. *J. Am. Chem. Soc.* **2007**, *129*, 10320–10321.

(4) Emmelius, M.; Pawlowsky, G.; Vollmann, H. W. *Angew. Chem., Int. Ed. Engl.* **1989**, *28*, 1445–1471.

(5) Ajayaghosh, A. *Acc. Chem. Res.* **2005**, *38*, 449–459.

(6) Basheer, M. C.; Alex, S.; Thomas, K. G.; Suresh, C. H.; Dasa, S. *Tetrahedron* **2006**, *62*, 605–610.

(7) Ramaiah, D.; Joy, A.; Chandasekhar, N.; Eldho, N. V.; Das, S.; George, M. V. *Photochem. Photobiol.* **1997**, *65*, 783–790.

(8) Ramaiah, D.; Eckert, I.; Arun, K. T.; Weidenfeller, L.; Epe, B. *Photochem. Photobiol.* **2002**, *76*, 672–677.

(9) Reis, V.; Serrano, J. P. C.; Almeida, P.; Santos, P. F. *Synlett.* **2002**, 1617–1620.

(10) Juzeniene, A.; Peng, Q.; Moan, J. *Photochem. Photobiol. Sci.* **2007**, *6*, 1234–1245.

(11) MacDonald, I. J.; Dougherty, T. J. *J. Porphyrins Phthalocyanines* **2001**, *5*, 105–129.

(12) Van Tenten, Y.; Schuitmaker, H. J.; De Wolf, A.; Willekens, B.; Vrensen, G. F. J. M.; Tassignon, M. J. *Exp. Eye Res.* **2001**, *72*, 41–48.

(13) Dolmans, D. E. J. G. J.; Fukumura, D.; Jain, R. K. *Nat. Rev. Cancer* **2003**, *3*, 380–387.

(14) Dougherty, T. J.; Gomer, C. J.; Henderson, B. W.; Jori, G.; Kessel, D.; Korbelik, M.; Moan, J.; Peng, Q. *J. Natl. Cancer Inst.* **1998**, *90*, 889–905.

(15) Bonnett, R. In *Chemical Aspects of Photodynamic Therapy*, Gordon & Breach Science Publishers: Amsterdam, 2000; pp 1−289.

(16) DeRosa, M. C.; Crutchley, R. J. *Coord. Chem. Rev.* **2002**, *233−234*, 351–371.

(17) Schweitzer, C.; Schmidt, R. *Chem. Rev.* **2003**, *103*, 1685–1757.

(18) Schmidt, R. *Photochem. Photobiol. A* **2006**, *82*, 1161–1177.

(19) Woodhams, J. H.; MacRobert, A. J.; Bown, S. G. *Photochem. Photobiol. A* **2007**, *6*, 1246–1256.

(20) Oleinick, N. L.; Morris, R. L.; Belichenko, I. *Photochem. Photobiol. A* **2002**, *1*, 1–21.

(21) Jyothish, K.; Arun, K. T.; Ramaiah, D. *Org. Lett.* **2004**, *22*, 3965–3968.

(22) Sternberg, E. D.; Dolphin, D.; Brückner, C. *Tetrahedron* **1998**, *54*, 4151–4202.

(23) Wainwright, M. *Chem. Soc. Rev.* **1996**, *25*, 351–359.

(24) Wöhrle, D.; Hirth, A.; Bogdahn-Rai, T.; Schnurpfeil, G.; Shopova, M. *Chem. Bull.* **1998**, *47*, 807–816.

(25) Sharman, W. M.; Allen, G. M.; VanLier, J. E. *Drug Discovery Today* **1999**, *4*, 507–517.

(26) Young, S. W.; Woodbourn, K. W.; Wright, M. *Photochem. Photobiol. A* **1996**, *63*, 892–897.

(27) Chowdhary, R. K.; Ratkay, L. G.; Canaan, A. J.; Waterfield, J. D.; Richter, A. M.; Levy, J. G. *Biopharm. Drug Dispos.* **1998**, *19*, 395–400.

(28) Gorman, A.; Killoran, J.; O'Shea, C.; Kenna, T.; Gallagher, W. M.; O'Shea, D. F. *J. Am. Chem. Soc.* **2004**, *126*, 10619–10631.

(29) Killoran, J.; Allen, L.; Gallagher, J. F.; Gallagher, W. M.; O'Shea, D. F. *Chem. Commun.* **2002**, *17*, 1862–1863.

(30) Yukruk, F.; Dogan, A. L.; Canpinar, H.; Guc, D.; Akkaya, E. U. *Org. Lett.* **2005**, *7*, 2885–2887.

(31) Beverina, L.; Crippa, M.; Landenna, M.; Ruffo, R.; Salice, P.; Silvestri, F.; Versari, S.; Villa, A.; Ciaffoni, L.; Collini, E.; Ferrante, C.; Bradamante, S.; Mari, C. M.; Bozio, R.; Pagani, G. A. *J. Am. Chem. Soc.* **2008**, *130*, 1894–1902.

(32) Ramaiah, D.; Eckert, I.; Arun, K. T.; Weidenfeller, L.; Epe, B. *Photochem. Photobiol. A* **2004**, *79*, 99–104.

(33) Santos, P. F.; Reis, L. V.; Almeida, P.; Oliveira, A. S.; Vieira Ferriera, L. F. *J. Photochem. Photobiol. A* **2003**, *160*, 159–161.

(34) Arunkumar, E.; Sudeep, P. K.; Kamat, P. V.; Nolla, B. C.; Smith, B. D. *New J. Chem.* **2007**, *31*, 677–683.

(35) Bonnett, R.; Motevalli, M.; Siu, J. *Tetrahedron* **2004**, *60*, 8913–8918.

(36) Beverina, L.; Abbotto, A.; Landenna, M.; Cerminara, M.; Tubino, R.; Meinardi, F.; Bradamante, S.; Pagani, G. A. *Org. Lett.* **2005**, *7*, 4257–4260.

(37) Casida, M. E. In *Recent Advances in Density Functional Methods*; Chong, D. P. Ed.; World Scientific: Singapore, 1995; Part I, pp 155−192.

(38) Christiansen, O.; Koch, H.; Jørgensen, P. *Chem. Phys. Lett.* **1995**, *243*, 409–418.

(39) Ahlrichs, R.; Bär, M.; Häser, M.; Horn, H.; Kölmel, C. *Chem. Phys. Lett.* **1989**, *162*, 165–169.

(40) Perdew, J. P.; Burke, K.; Ernzerhof, M. *Phys. Rev. Lett.* **1996**, *77*, 3865–3868.

(41) Perdew, J. P.; Ernzerhof, M.; Burke, K. *J. Chem. Phys.* **1996**, *105*, 9982–9985.

(42) Schäfer, A.; Horn, H.; Ahlrichs, R. *J. Chem. Phys.* **1992**, *97*, 2571–2577.

(43) Bauernschmitt, R.; Ahlrichs, R. *Chem. Phys. Lett.* **1996**, *256*, 454–464.

(44) Hättig, C.; Weigend, F. *J. Chem. Phys.* **2000**, *113*, 5154–5161.

(45) Hättig, C.; Hald, K. *Phys. Chem. Chem. Phys.* **2002**, *4*, 2111–2118.

(46) Schäfer, A.; Huber, C.; Ahlrichs, R. *J. Chem. Phys.* **1992**, *100*, 5829–5835.

(47) Dunning, T. H. *J. Chem. Phys.* **1989**, *90*, 1007–1023. http://bse.pnl.gov/bse/portal (accessed January, 2009).

(48) Quartarolo, A. D.; Russo, N.; Sicilia, E. *Chem.— Eur. J.* **2006**, *12*, 6797–6803.

(49) Jacquemin, D.; Perpete, E.; Scuseria, G. E.; Ciofini, I.; Adamo, C. *J. Chem. Theory Comput.* **2008**, *4*, 123–135.

(50) Lanzo, I.; Quartarolo, A. D.; Russo, N.; Sicilia, E. *Photochem. Photobiol. A* **2009**, *8*, 386–390.

(51) Jacquemin, D.; Perpete, E.; Ciofini, I.; Adamo, C. *Acc. Chem. Res.* **2009**, *42*, 326–332.

(52) Klamt, A.; Schüürmann, G. *J. Chem. Soc. Perkin Trans. 2* **1993**, *5*, 799–805.

(53) Tomasi, J.; Mennucci, B.; Cammi, R. *Chem. Rev.* **2005**, *105*, 2999–3094.

(54) Turro, N. J. In *Modern Molecular Photochemistry*; University Science Books, 1991, pp 1−292.

(55) Gouterman, M.; Khalil, G. *J. Mol. Spectrosc.* **1974**, *53*, 88–100.

(56) Radziszewski, J. G.; Waluk, J.; Nepras, M.; Michl, J. *J. Phys. Chem.* **1991**, *95*, 1963–1969.

(57) Tawada, Y.; Tsuneda, T.; Yanagisawa, S. *J. Chem. Phys.* **2004**, *18*, 8425–8433.

(58) Vydrov, O. A.; Scuseria, G. E. *J. Chem. Phys.* **2006**, *125*, 234109.

(59) Chai, J.; Head-Gordon, M. *J. Chem. Phys.* **2008**, *128*, 84106.

CT900199J